Turkish Journal of Science & Technology
18(2), 363-378, 2023

Research Paper
https://doi.org/10.55525/tjst.1277586

Numerical Investigation of Heat Transfer on Hot and Cold Sides of a Thermoelectric Generator Using Heat Sinks

Enes KILINÇ[1*]
[1] Department of Mechanical Engineering, Faculty of Engineering, Karabük University, Karabük, Türkiye
[*1] eneskilinc@karabuk.edu.tr

(Geliş/Received: 05/04/2023; Kabul/Accepted: 16/08/2023)

Abstract: This study represents Computational Fluid Dynamics (CFD) analyses to improve the heat transfer on the two sides of a thermoelectric generator (TEG) by utilizing heat sinks to recover the waste heat of hot air. In this respect, the temperature difference between the hot and cold sides of the TEG, the heat transfer rate on the hot and cold sides and the pressure drop between the inlet and outlet of the hot and cold air are investigated for varying hot air inlet temperature and *Re* number in terms of improving the heat transfer and accordingly the output power of the TEG. According to the numerical results, the maximum temperature difference between the hot and cold sides of the TEG concerning hot air inlet temperature of 600 °C and Re number of 16800 is specified as 418.9 °C and 478.1 °C, respectively. In terms of heat transfer, maximum heat transfer rate on the hot side for hot air inlet temperature of 600 °C and Re number of 16800 is specified as 180.4 W and 205.1 W, respectively, while the maximum heat transfer rate on the cold side is specified as 168.0 W and 192.6 W. The maximum pressure drop occurs as 304.4 Pa for the *Re* number of 16800. As a result, increasing hot air inlet temperature and *Re* number yields an increase in the temperature difference, the heat transfer rate on the hot side, and the heat transfer rate on the cold side. Besides, pressure drop increases with increasing *Re* number.

Keywords: Thermoelectric generator, waste heat, CFD modeling, temperature distribution, heat transfer.

Isı Kuyuları Kullanılarak Bir Termoelektrik Jeneratörün Sıcak ve Soğuk Yüzeyindeki Isı Transferinin Sayısal Olarak İncelenmesi

Öz: Bu çalışmada, sıcak havanın atık ısısını geri kazanmak için ısı kuyuları kullanılarak bir termoelektrik jeneratörün (TEG) iki yüzeyindeki ısı transferinin iyileştirilmesi için yapılan Hesaplamalı Akışkanlar Dinamiği (HAD) analizleri sunulmaktadır. Bu bağlamda, ısı transferinin ve buna bağlı olarak TEG'in çıkış gücünün iyileştirilmesi için TEG'in sıcak ve soğuk yüzeyleri arasındaki sıcaklık farkı, sıcak ve soğuk yüzeyindeki ısı transfer hızı ve sıcak ve soğuk havanın giriş ve çıkışı arasındaki basınç düşüşü değişken sıcak hava giriş sıcaklığı ve *Re* sayısı için incelenmiştir. Sayısal sonuçlara göre, 600 °C sıcak hava giriş sıcaklığı ve 16800 *Re* sayısı için maksimum sıcaklık farkı sırasıyla 418,9 °C ve 478,1 °C olarak belirlenmiştir. Isı transferi açısından, 600 °C sıcak hava giriş sıcaklığı ve 16800 *Re* sayısı için sıcak yüzeydeki maksimum ısı transfer hızı sırasıyla 180,4 W ve 205,1 W olarak belirlenirken soğuk yüzeydeki maksimum ısı transfer hızı 168,0 W ve 192,6 W olarak belirlenmiştir. Maksimum basınç düşüşü, 16800 *Re* sayısı için 304,4 Pa olarak gerçekleşmiştir. Sonuç olarak, artan sıcak hava giriş sıcaklığı ve *Re* sayısı, sıcaklık farkı ve sıcak ve soğuk yüzeylerdeki ısı transfer hızlarında artışa neden olmuştur. Ayrıca, basınç düşüşü, artan *Re* sayısı ile artmıştır.

Anahtar kelimeler: Termoelektrik jeneratör, atık ısı, CFD modelleme, sıcaklık dağılımı, ısı transferi.

Nomenclature

A_{TEG}	Total TE leg cross-sectional area of the TEG	T	Temperature
c_p	Specific heat	T_c	Cold side temperature of the TEG
$C_{1\varepsilon}$	Constant	T_{ci}	Cold air inlet temperature
$C_{2\varepsilon}$	Constant	T_{co}	Cold air outlet temperature
$C_{3\varepsilon}$	Constant	T_h	Hot side temperature of the TEG
G_k	Generation of the turbulence kinetic energy due to mean velocity gradient	T_{hi}	Hot air inlet temperature
		T_{ho}	Hot air outlet temperature
G_b	Generation of the turbulence kinetic energy due to buoyancy	V	Velocity
		Y_M	Contribution of the fluctuating dilatation to the overall dissipation
k	Thermal conductivity		
k	Turbulence kinetic energy	zT	Figure of merit
P	Pressure	ΔP	Pressure drop

* Corresponding author: eneskilinc@karabuk.edu.tr. ORCID Number of authors: [1] 0000-0002-9585-998X

$\dot{q}_c$	Heat transfer rate on the cold side of the TEG	ΔT	Temperature difference
		ε	Dissipation rate
$\dot{q}_h$	Heat transfer rate on the hot side of the TEG		
P	Output power of the TEG	μ_t	Turbulent viscosity
Re	Reynolds number	ρ	Density
S_k	User defined source term	σ_k	Turbulent Prandtl number for k
S_ε	User defined source term	σ_ε	Turbulent Prandtl number for ε

1. Introduction

Thermoelectric (TE) devices are novel waste heat recovery solutions that convert heat energy directly into electrical energy [1,2]. They have been studied for industrial areas such as space applications, photovoltaic (PV) technology, the automotive industry, and power plants [3]. Applying temperature difference between the hot and cold sides of TE devices yields voltage occurrence and electrical power generation, known as the Seebeck effect [4]. TE devices are advantageous in power generation in terms of having no moving parts, being compact, quiet, environmentally friendly, and maintenance-free [5]. However, reasonably low heat-to-electricity conversion efficiencies of TE devices are the major task in improving waste heat recovery using TEs [6].

For the last decades, many researchers have focused on improving the figure of merit (zT) of TE materials, optimizing the design of thermoelectric generators (TEGs), and improving operating conditions of TEGs in terms of increasing the conversion efficiency of TEGs [7]. Regarding improving operating conditions, TEGs have been modeled and characterized to specify the effects of the crucial parameters on the performance of TEGs [8]. Therefore, heat transfer enhancement on the hot and cold sides of the TE modules is crucial for the performance of TEGs [7]. Within this scope, Li et al. numerically investigated the effects of leg length and heat radiation on the thermal performance of a TEG sandwiched between cold and hot blocks under steady-state and transient conditions [9]. They have found that numerical and experimental performance curves agree, and the radiation heat transfer and the length of TEG's leg are negligible on the thermal performance of the TEG. Miao et al. investigated the effect of the geometric structure of a TE module on power generation [10]. They have stated that the conversion efficiency changes with the change in heat absorption of the TE module. As a result, the conversion efficiency of the TE module decreases when the heat absorption is higher. Nour Eddine et al. investigated the effect of clamping pressure on the performance of two commercial TE modules for marine applications [11]. They have obtained conversion efficiencies in the range of 0.05-0.35% and 0.26-0.4% for the $Si_{80}Ge_{20}$ and Bi_2Te_3 TE modules, respectively, for a Diesel engine exhaust temperature of 380 °C. In their other work, Nour Eddine et al. established a model to investigate a TEG for waste heat recovery from the exhaust gas of an automotive engine [12]. They have reached a maximum generated TEG power of 42 W for 671 K of TEG hot side temperature and 354 K of cold side temperature.

Gürbüz et al. designed a three-layer sandwich-type TEG consisting of two cooling heat exchangers placed on both sides of the middle rectangular exhaust heat exchanger coupled to the exhaust path in a propane-fueled spark-ignition (SI) engine. They performed both experimental and computational fluid dynamics analyses to visualize both the cold and hot surface temperatures of the TEMs. According to the results, electrical power of the TEG with propane is higher in the range of 11.5–12.1% compared to the TEG without propane in the 1500–5000 rpm range of the SI engine in a good correlation between the experimental and numerical findings, varying between 3% and 15% with the engine speed [13]. In another study, Topalcı et al. developed a theoretical model with Matlab/Simulink of a thermoelectric generator used for waste heat recovery in a spark ignition (SI) engine. As a result, the DC electrical power production with the Matlab/Simulink model of the TEG changed in the range of 6.36-50.96 W for the engine speed range of 1500-4000 rpm [14]. Kunt et al. designed a waste heat recovery system with a thermoelectric generator for the exhaust system of a motorcycle engine with a cylinder volume of 50 cc [15]. The maximum recovery power has been found as 2.05 W at an engine speed of 6000 r/min and the maximum system efficiency has been found as 2.41% at an engine speed of 4000 r/min. Schwurack et al. considered inner heat losses in a TEG system for high-temperature applications [16]. As a result of the optimization study, total power output has been increased by 0.56%. Akçay et al. performed a numerical analysis of a 3-layer TEG consisting of a middle exhaust heat exchanger and two cooling water heat exchangers placed on both surfaces of the middle exhaust heat exchanger using computational fluid dynamics. As a result, it was found that the temperature difference increased by 32.45% by dividing the internal volume of the hot heat exchanger into two equal parts with a separator plate and the temperature difference increased by an additional 18.79% by adding flow diverter fins on the separator plate surfaces [17]. Ökmen et al. optimized hot-side heat exchangers with different fin numbers and arrangements in terms of surface temperature and temperature distribution in a thermoelectric

generator where electrical energy is generated from the exhaust waste heat energy of a spark ignition engine using the computational fluid dynamics [18]. In addition, Wang et al. constituted a mathematical model for harvesting the heat energy of vehicle exhaust gas through a TEG to investigate the effects of exhaust gas mass flow rate, temperature and mass flow rate of different coolants, and convection heat transfer coefficient [19].

In this study, the effects of *Re* number and hot air inlet temperature (T_{hi}) on the temperature difference (ΔT) between the hot and cold sides of a TEG, on the heat transfer rate on the hot ($\dot{q}_h$) and cold sides ($\dot{q}_c$) of the TEG, and on the pressure drop (ΔP) between the inlet and outlet of the hot and cold air were numerically investigated in terms of heat recovery from hot air. In the literature, there are few studies which focus on the heat transfer analysis of both hot and cold sides of the TEG. Besides, operating temperature of the TEGs are within low temperature range. Within this scope, hot air inlet temperatures ranged between 200-600 °C and *Re* numbers for the hot and cold air varied between 5600-18600, which point out the originality of the study. Hot air as the hot fluid and cold air as the cold fluid are modeled to flow in a counter-current manner on the hot and cold sides of the TE module, respectively. Temperature distributions in the hot and cold air, $\dot{q}_h$, $\dot{q}_c$, ΔP and ΔT were evaluated in terms of improving the operating conditions of TEGs.

2. Methodology

2.1. Physical Configuration

The objective of this study is to utilize heat energy in terms of generating electricity using TEG. In this respect, ΔT, $\dot{q}_h$, $\dot{q}_c$, and ΔP of a TEG are investigated in terms of improving the output power of the TEG. The TEG model consists of a TEG, two heat sinks on the hot and cold sides of the TEG, and hot and cold air as the fluids. To increase the output power of the TEG, one side of the TEG is heated by hot air, while the other side is cooled by cold air. Hot and cold air flowing over the hot and cold sides of the TEG are modeled to flow in a counter-current manner to increase the heat transfer. A heat sink with straight fins made of aluminum is used to enhance the heat transfer on both sides. **Figure 1** illustrates the physical model of the study, including hot air, cold air, heat sinks, and the TEG. The TEG used in the model comprises eight pairs of p- and n-type legs made of $Ca_{2.5}Ag_{0.3}Eu_{0.2}Co_4O_9$ and $Ca_{2.96}Dy_{0.02}Ho_{0.02}MnO_3$, respectively. Dimensions of the TEG are 44 mm x 44 mm x 7 mm. Accordingly, the base dimension of the heat sinks is 44 mm x 44 mm, and the height of the heat sink is 48 mm (**Figure 2**). Hot and cold air passes through the heat sinks. Solid and fluid properties used in the model are constant and are given in **Table 1**.

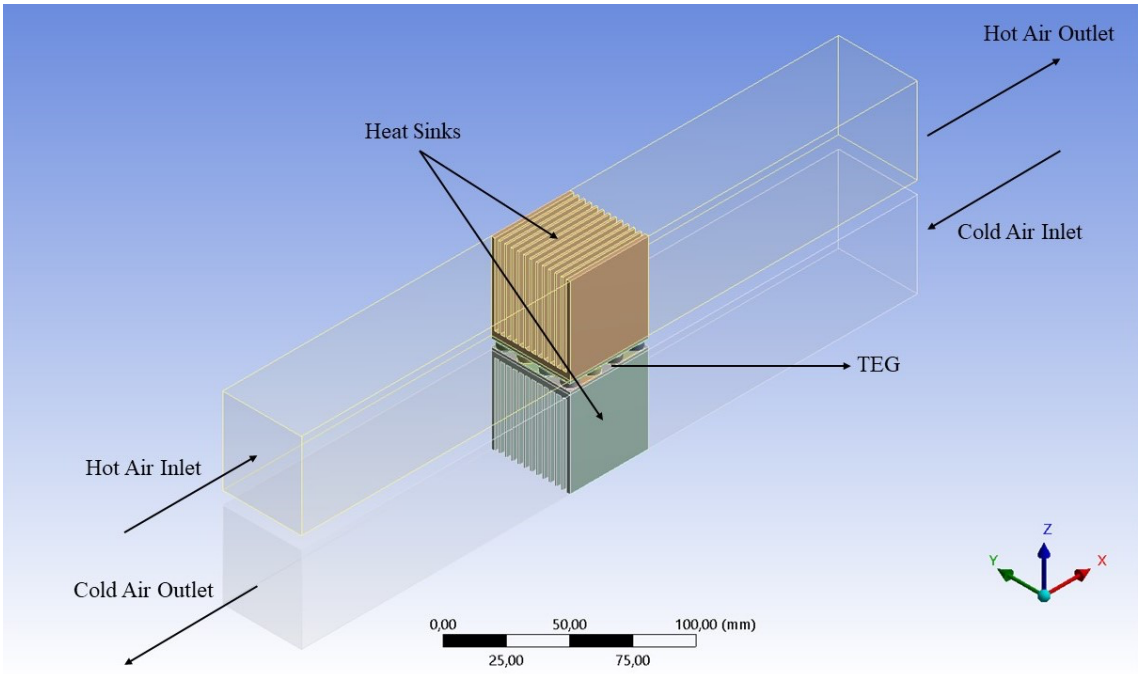

Figure 1. Physical model and boundary conditions of the TEG model.

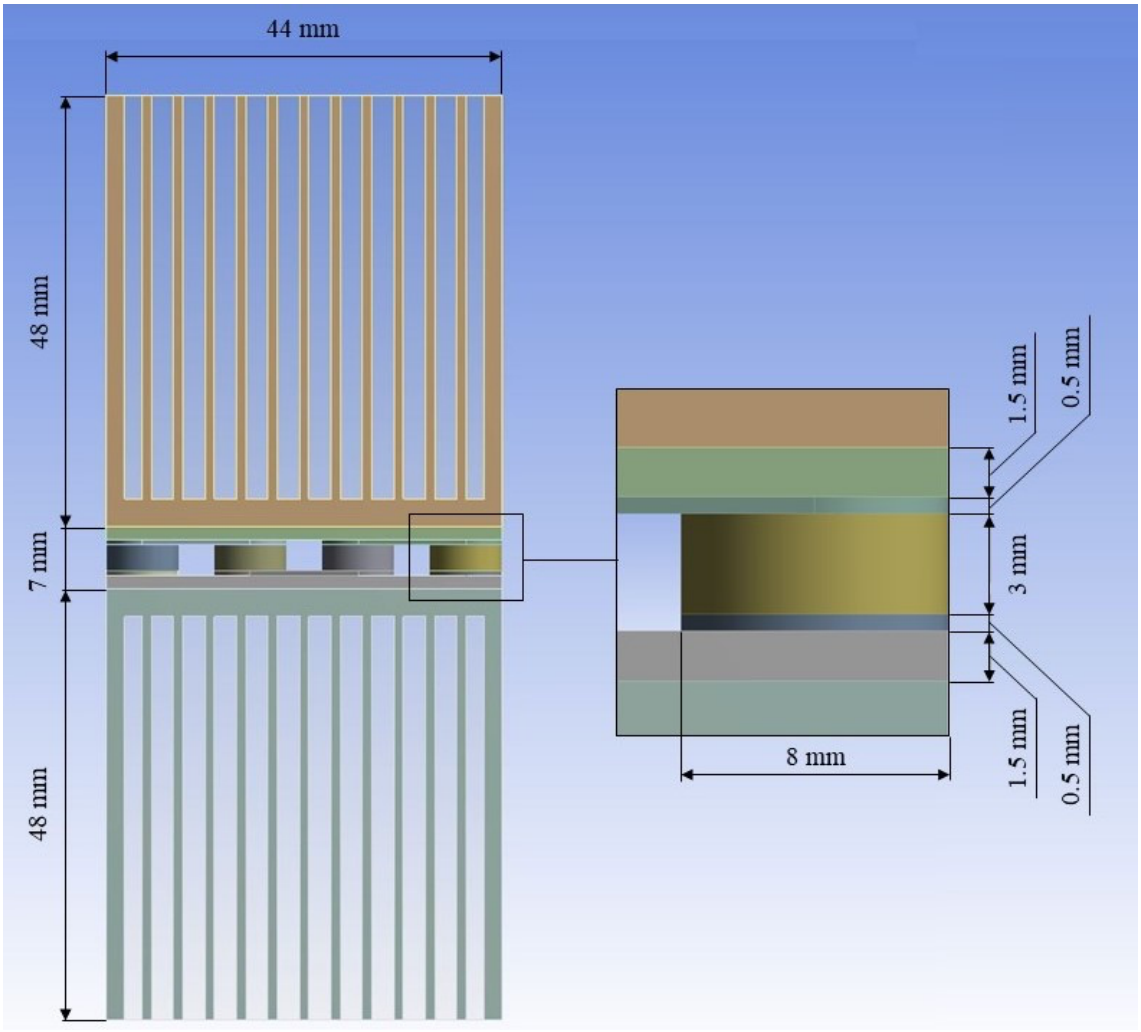

Figure 2. Dimensions of the TEG and the heat sinks in the model.

2.2. Turbulence Model and Boundary Conditions

Hot and cold flows in the model are designed to be three-dimensional, steady, and turbulent. The flow is assumed to be incompressible, and the fluid properties are assumed to be constant. The standard k-ε model is applied for the turbulent flow characteristics. The related governing equations and the turbulent kinetic energy are given as follows. Continuity equation is given as

$$\nabla.\left(\rho\vec{V}\right) = 0 \tag{1}$$

where ρ is the density and V is the velocity of the fluid. Momentum equation is expressed as

$$\rho\vec{V}.\nabla\vec{V} = -\nabla P + \nabla.\left[\mu\left(\nabla\vec{V} + \left(\nabla\vec{V}\right)^{T}\right)\right] \tag{2}$$

where P is the pressure. Energy equation is given as

Table 1. Material properties used in the TEG model.

Material	Definition	Value
Air	Thermal Conductivity	0.0242 W/m·K
	Specific Heat	1006.43 J/kg·K
	Density	1.225 kg/m^3
	Viscosity	1.7894x10^{-5} kg/m·s
Heat Sink	Thermal Conductivity	218 W/m·K
	Specific Heat	900 J/kg·K
	Density	2690 kg/m^3
P-type Leg	Thermal Conductivity	2.49 W/m·K
	Specific Heat	735 J/kg·K
	Density	3870 kg/m^3
N-type Leg	Thermal Conductivity	0.73 W/m·K
	Specific Heat	843 J/kg·K
	Density	2470 kg/m^3
Alumina Plate	Thermal Conductivity	25 W/m·K
	Specific Heat	880 J/kg·K
	Density	3720 kg/m^3
Silver Conductor	Thermal Conductivity	429 W/m·K
	Specific Heat	237 J/kg·K
	Density	10497 kg/m^3

$$\nabla.\left(\vec{V}\rho c_p T\right) = \nabla.(k\nabla T) + S_g \tag{3}$$

where c_p is the specific heat, k is the thermal conductivity, and T is the temperature of the fluid. Turbulence kinetic energy k is expressed as

$$\frac{\partial}{\partial x_i}(\rho k u_i) = \frac{\partial}{\partial x_j}\left[\left(\mu + \frac{\mu_t}{\sigma_k}\right)\frac{\partial_k}{\partial x_j}\right] + G_k + G_b - \rho\varepsilon - Y_M + S_k \tag{4}$$

where Y_M is the contribution of the fluctuating dilatation to the overall dissipation. Dissipation rate ε is given as

$$\frac{\partial}{\partial x_i}(\rho\varepsilon u_i) = \frac{\partial}{\partial x_j}\left[\left(\mu + \frac{\mu_t}{\sigma_\varepsilon}\right)\frac{\partial_\varepsilon}{\partial x_j}\right] + C_{1\varepsilon}\frac{\varepsilon}{k}(G_k + C_{3\varepsilon}G_b) - C_{2\varepsilon}\rho\frac{\varepsilon^2}{k} + S_\varepsilon \tag{5}$$

In these equations, G_k and G_b are the generation of the turbulence kinetic energy due to mean velocity gradient and buoyancy. Turbulent viscosity, μ_t is calculated as $\mu_t = \rho C_\mu \frac{k^2}{\varepsilon}$. Constants of $C_{1\varepsilon} = 1.44$, $C_{2\varepsilon} = 1.92$, and $C_{3\varepsilon} = 0.09$, and turbulent Prandtl numbers of $\sigma_k = 1.0$ and $\sigma_\varepsilon = 1.3$ are determined experimentally. S_k and S_ε are user defined source terms [20].

The walls of the hot and cold air and outside surfaces of the heat sinks are modeled as adiabatic, and the heat transfer coefficient of 10 W/m·K is defined on the outside surfaces of the TEG. The no-slip boundary condition is applied on the surfaces of the heat sinks. Heat radiation is neglected in the whole model. Regarding accuracy and minimizing the simulation time, the mesh structure is optimized, and the number of grids for the model is 10,500,000. Body sizing applied to the TEG and the heat sinks are most influential in the number of grids. The TEG model is designed in Ansys DesignModeler, and Ansys Fluent is used to determine the temperature distributions in the hot and cold air, $\dot{q}_h$, $\dot{q}_c$, ΔP, and ΔT. Boundary conditions are demonstrated in **Figure 1**.

To improve the $\dot{q}_h$ and ΔT of the TEG, T_{hi} is altered as 200 °C, 300 °C, 400 °C, 500 °C, and 600 °C while the cold air inlet temperature (T_{ci}) and *Re* number are held constant at 25 °C and 5600, respectively. *Re* numbers for the hot and cold air are assumed to be the same and varied as 5600, 8400, 11200, 14000, and 16800 after specifying the optimum T_{hi} to enhance $\dot{q}_h$. During the analyses, T_{hi} and T_{ci} are held constant at 600 °C and 25 °C, respectively. Outlet pressures of the hot and cold air are specified as the atmospheric pressure.

3. Results and Discussion

3.1. Temperature Distribution in the Hot and Cold Air

Temperature distributions in the hot and cold air were obtained as a result of CFD analyses concerning different T_{hi} and *Re* numbers. **Figure 3** illustrates the temperature distribution in the hot and cold air for T_{hi}. According to the figure, T_{hi} decreases when the hot air flows through the heat sink, while T_{ci} increases when the cold air flows through the heat sink. The reason for the decrease in T_{hi} and the increase in T_{ci} is the heat transfer to the TEG by the heat sink. When **Figure 3a - Figure 3e** are investigated, the difference between T_{hi} and hot air outlet temperature (T_{ho}) increases with increasing T_{hi} as the difference between T_{ci} and cold air outlet temperature (T_{co}), which leads to the increase in the heat transfer between the heat sinks and the TEG. Accordingly, the air temperature decreases on the surfaces of the heat sink fins for the hot air. In contrast, the air temperature increases on the surfaces of the heat sink fins for the cold air due to the convection heat transfer between the air and the heat sink. It can be seen from the figures that the hot air temperature is the lowest at the surfaces of the outside fins of the heat sinks due to the convection boundary condition defined on the outside surfaces of the heat sinks. Similarly, the temperature of the cold air is the highest at the surfaces of the outside fins of the heat sinks due to the convection boundary condition defined on the outside surfaces of the heat sinks. For T_{hi} = 600 °C, temperatures of the hot and cold air at the outlet of the heat sinks are obtained as 592 °C and 33 °C, respectively.

When the temperature distribution in the hot and cold air concerning different *Re* numbers is investigated, it can be seen from **Figure 4** that similar observations are obtained with the effects of the T_{hi} on the temperature distribution. According to **Figure 4a - Figure 4e**, T_{hi} decreases when the hot air flows through the heat sink, while T_{ci} increases when the cold air flows through the heat sink. It can be seen from the figures that an increase in *Re* number yields a significant increase in T_{ho} while yields a significant decrease in T_{co}. However, this effect reduces the temperature differences between T_{hi} and T_{ho} as the temperature difference between T_{ci} and T_{co}, which leads to a decrease in the heat transfer between the heat sinks and the TEG. As a result, temperature of the hot air at the outlet of the heat sink increased and reached to the value of 598 °C, while temperature of the cold air at the outlet of the heat sink decreased to 27 °C.

3.2. Velocity Distribution in the Hot and Cold Air

Velocity distributions in the hot and cold air are presented in **Figure 5a – Figure 5e** with respect to the Re numbers. Hot and cold air enters the flow channels at velocities of 5 m/s, 7.5 m/s, 10 m/s, 12.5 m/s, and 15 m/s for the *Re* numbers of 5600, 8400, 11200, 14000, and 16800, respectively. According to the figure, velocities of the hot and cold air are equal to zero due to the no-slip boundary condition on the outer surfaces of the hot and cold air. In addition, velocities of the hot and cold air increase due to the steady flow while passing through the fins of heat sinks since the flow area decreases at these regions. As it can be seen form the figures that maximum velocity is obtained at the flow axis, decreasing towards the outer surfaces of the hot and cold air. Velocities of the hot and cold air increases when the *Re* number increases and become maximum between the fins of the heat sinks. The velocities of the hot and cold air increase up to 10 m/s, 15 m/s, 20 m/s, 25 m/s, and 30 m/s, for *Re* numbers of 5600, 8400, 11200, 14000, and 16800, respectively. The increase in the velocity yields an increase in the heat transfer between the heat sinks and the fluids resulting a significant increase in hot air temperature and a significant decrease in cold air temperature. Velocity contours for the hot and cold air shows similar characteristics since the *Re* numbers, flow geometry, and flow parameters are the same for both fluids. The only variable which has a negligible effect on the velocity is the temperature of the hot and cold fluid.

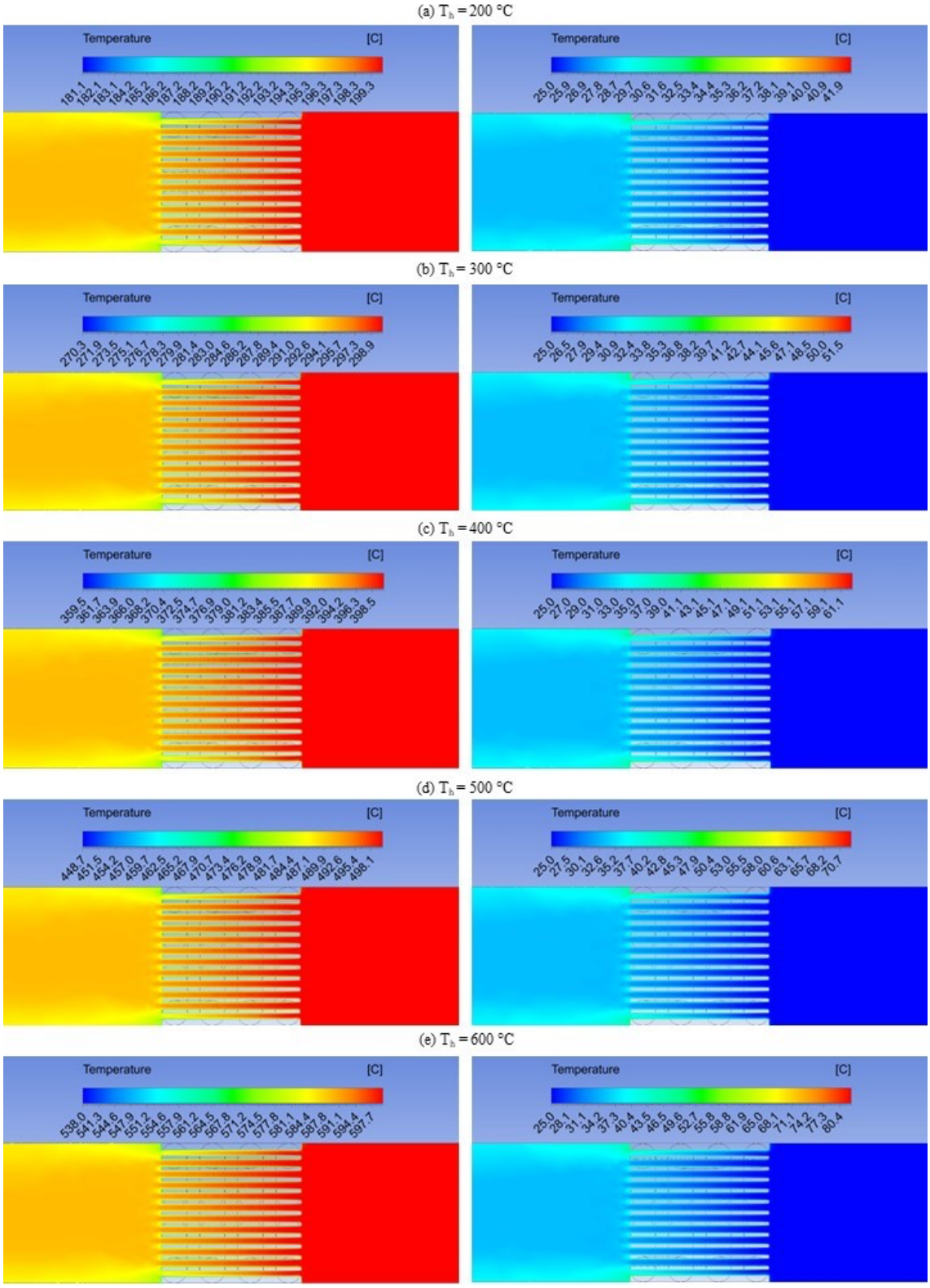

Figure 3. Temperature distribution in the hot and cold air for T_{hi} (a) T_{hi} = 200 °C (b) T_{hi} = 300 °C (c) T_{hi} = 400 °C (d) T_{hi} = 500 °C (e) T_{hi} = 600 °C.

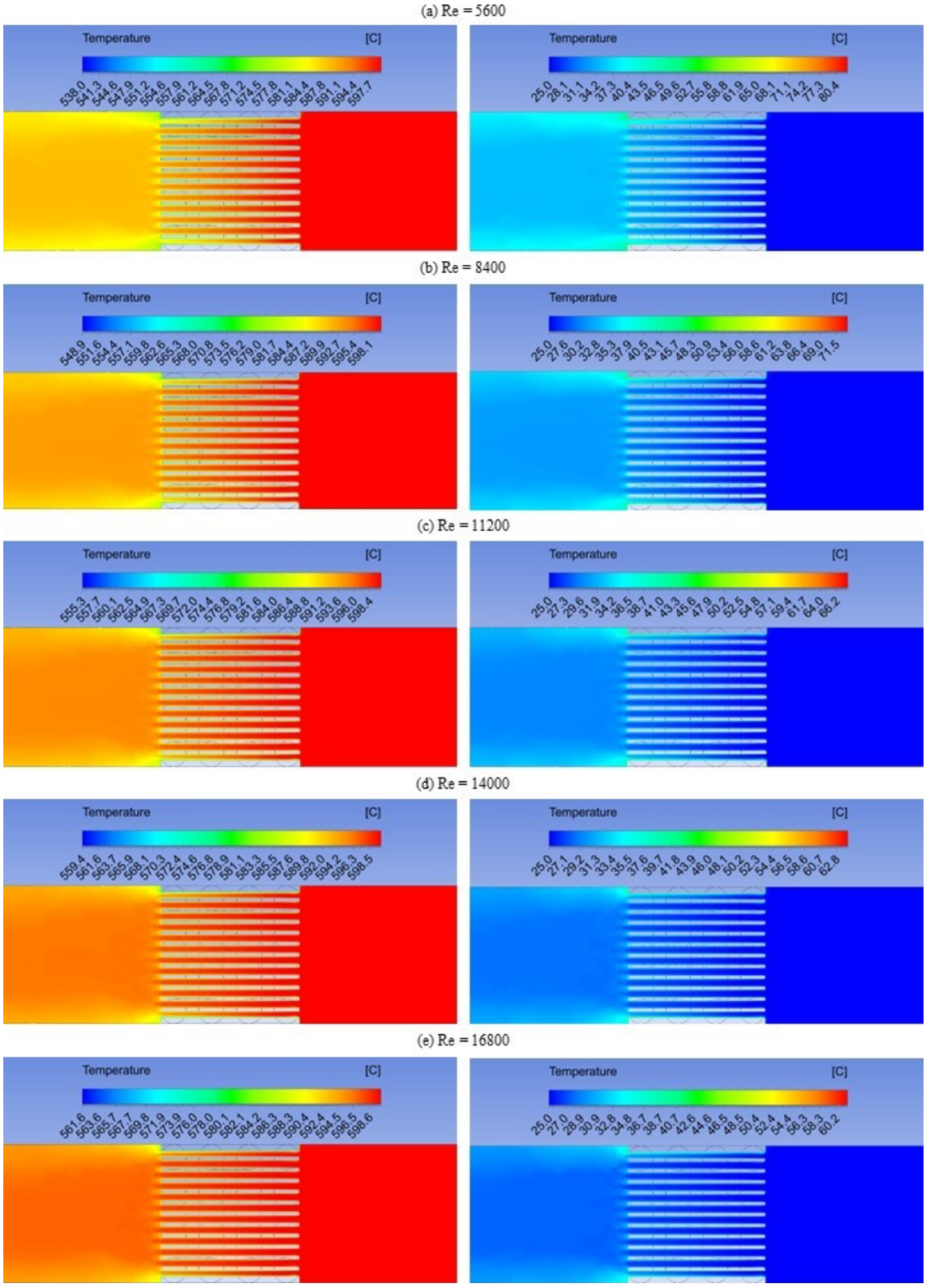

Figure 4. Temperature distribution in the hot and cold air for (a) *Re* = 5600 (b) *Re* = 8400 (c) *Re* = 11200 (d) *Re* = 14000 (e) *Re* = 16800.

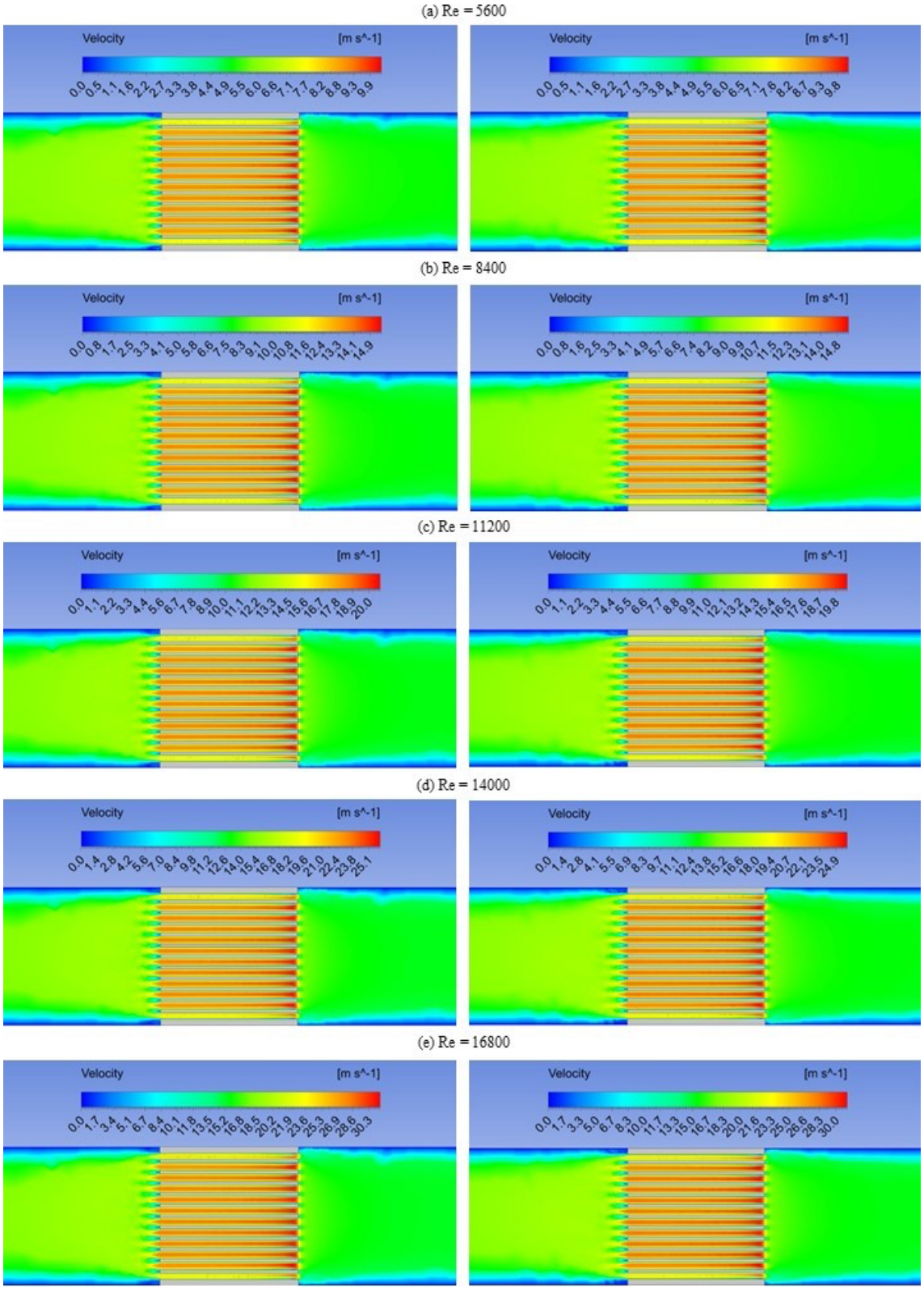

Figure 5. Velocity distribution in the hot (on the left) and cold air (on the right) for (a) *Re* = 5600 (b) *Re* = 8400 (c) *Re* = 11200 (d) *Re* = 14000 (e) *Re* = 16800.

3.3. Temperature Difference Between Hot and Cold Sides of the TEG (ΔT)

The performance of TEGs is directly related to the ΔT. To increase the ΔT, the hot side temperature (T_h) and cold side temperature (T_c) of the TEG are investigated with respect to different T_{hi} and Re number. Since the temperature of the waste heat sources differs in the industry, T_{hi} of 200 °C, 300 °C, 400 °C, 500 °C, and 600 °C are applied in the analyses to obtain the highest ΔT. After obtaining the highest ΔT for T_{hi}, the Re number of the flow is varied as 5600, 8400, 11200, 14000, and 16800 to increase the ΔT further. **Figure 6** and **Figure 7** illustrate the T_h, T_c, and ΔT concerning T_{hi} and Re number, respectively. It can be seen from both figures that T_h increases with increasing T_{hi} and Re numbers. However, T_c increases with increasing T_{hi} while decreases with increasing Re number. The reason for this behavior is the convection heat transfer between hot and cold air and the heat sink. While the temperature increase in T_{hi} directly affects the T_h, the increase in Re number affects the surface temperature indirectly, including other flow parameters. This effect results in the linear variation in T_h, T_c, and ΔT concerning T_{hi}, whereas polynomial variation is confirmed with respect to the Re number.

According to both figures, ΔT increased with increasing T_{hi} and Re numbers. It can be noted that the Re number is effective on the ΔT in addition to T_{hi} to increase the ΔT further. The increase in the Re number yields an increase in the Nu number and the convection heat transfer coefficient. According to the results, T_h values are obtained as 175.4 °C, 261.3 °C, 347.3 °C, 433.2 °C, and 519.2 °C, while ΔT values are obtained as 127.4 °C, 200.3 °C, 273.2 °C, 346.0 °C, and 418.9 °C for T_{hi} of 200 °C, 300 °C, 400 °C, 500 °C, and 600 °C, respectively. Meanwhile, T_h values are obtained as 519.2 °C, 532.6 °C, 540.6 °C, 546.0 °C, and 550.0 °C, while ΔT values are obtained as 418.9 °C, 444.6 °C, 459.9 °C, 470.4 °C, and 478.1 °C for Re number of 5600, 8400, 11200, 14000, and 16800, respectively. As a result, maximum T_h with respect to T_{hi} of 600 °C and Re number of 16800 is specified as 519.2 °C and 550.0 °C, respectively, while maximum ΔT is specified as 418.9 °C and 478.1 °C. According to the results, T_h of 550 °C is higher than the results of Kim et al [21]. In their study, the maximum hot side temperature increased to 229 °C where the number of fin was eight. T_h in this study is higher than the study of Kim et al. since the number of fins, geometrical dimensions and boundary conditions are different.

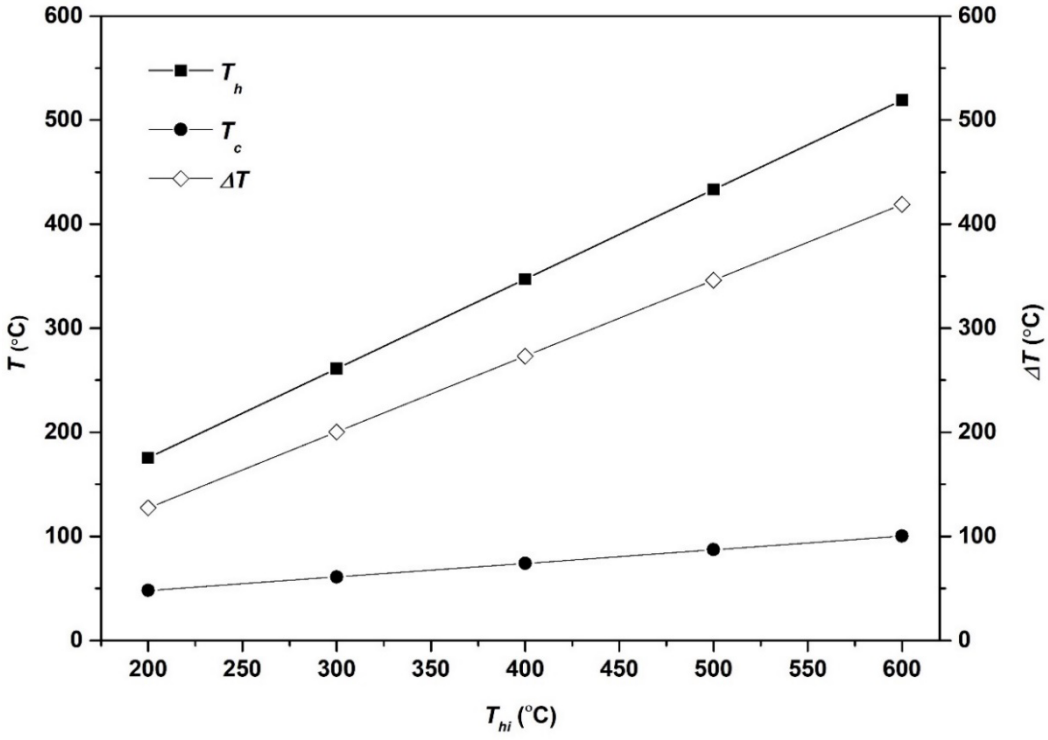

Figure 6. T_h, T_c, and ΔT of the TEG for T_{hi}.

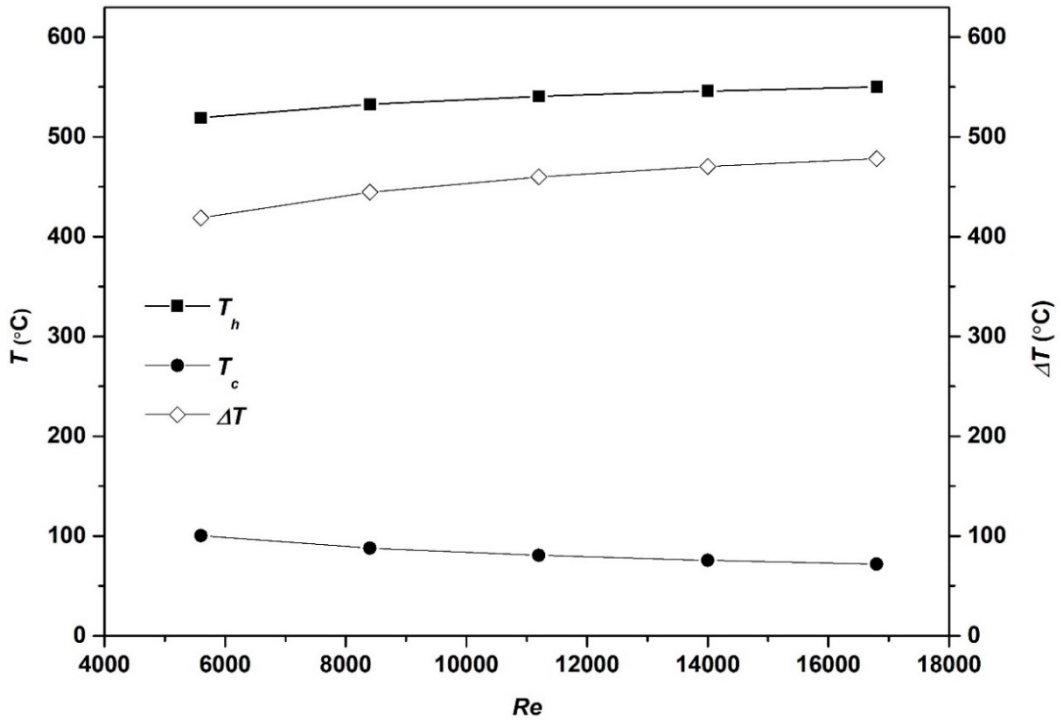

Figure 7. T_h, T_c, and ΔT of the TEG for *Re* number.

3.4. Heat Transfer Rate and Output Power of the TEG ($\dot{q}$, *P*)

Increasing $\dot{q}_h$ and $\dot{q}_c$ for the TEG means better heat transfer rates on two sides of the TEG and yields an increase in ΔT and the power generation performance of TEGs. In this study, $\dot{q}_h$ and $\dot{q}_c$ are investigated concerning different T_{hi} and *Re* numbers to increase the power generation performance of TEGs. Since the temperature of the waste heat sources differ in the industry, T_{hi} of 200 °C, 300 °C, 400 °C, 500 °C, and 600 °C are applied in the analyses to obtain the highest $\dot{q}_h$ and $\dot{q}_c$. After varying T_{hi} and obtaining the highest $\dot{q}_h$ and $\dot{q}_c$ for T_{hi}, the *Re* number of the flow is varied as 5600, 8400, 11200, 14000, and 16800 to increase the $\dot{q}_h$ and $\dot{q}_c$ further. **Figure 8** and **Figure 9** illustrate the $\dot{q}_h$ and $\dot{q}_c$ with respect to T_{hi} and *Re* number, respectively. It can be seen from both figures that $\dot{q}_h$ and $\dot{q}_c$ increase with increasing T_{hi} and *Re* numbers. While the temperature increase in T_{hi} directly affects the $\dot{q}_h$ and $\dot{q}_c$, the increase in *Re* number affects the $\dot{q}_h$ and $\dot{q}_c$ indirectly including other flow parameters. This effect results in the linear variation in $\dot{q}_h$ and $\dot{q}_c$ for T_{hi}, whereas polynomial variation is confirmed with respect to the *Re* number.

According to both figures, it can be noted that the *Re* number is effective on the $\dot{q}_h$ and $\dot{q}_c$ in addition to T_{hi} to further increase the $\dot{q}_h$ and $\dot{q}_c$. The increase in the *Re* number yields an increase in the Nu number and the convection heat transfer coefficient. According to the results, $\dot{q}_h$ values are obtained as 54.9 W, 86.2 W, 117.6 W, 149.0 W, and 180.4 W, while $\dot{q}_c$ values are obtained as 51.2 W, 80.4 W, 109.6 W, 138.8 W, and 168.0 W for T_{hi} of 200 °C, 300 °C, 400 °C, 500 °C, and 600 °C, respectively. Meanwhile, $\dot{q}_h$ values are obtained as 180.4 W, 191.1 W, 197.5 W, 201.8 W, and 205.1 W, while $\dot{q}_c$ values are obtained as 168.0 W, 178.7 W, 185.1 W, 189.4 W, and 192.6 W for *Re* numbers of 5600, 8400, 11200, 14000, and 16800, respectively. As a result, maximum $\dot{q}_h$ with respect to T_{hi} of 600 °C and *Re* number of 16800 are specified as 180.4 W and 205.1 W, respectively, while the maximum $\dot{q}_c$ is specified as 168.0 W and 192.6 W. In this study, $\dot{q}_h$ reached to the value of 192.6 W which is much higher than the study of Chen et al [20]. In their study, they obtained a lower $\dot{q}_h$ of 85.85 W for the plate fins due to the difference in number of fins, geometrical dimensions, and boundary conditions.

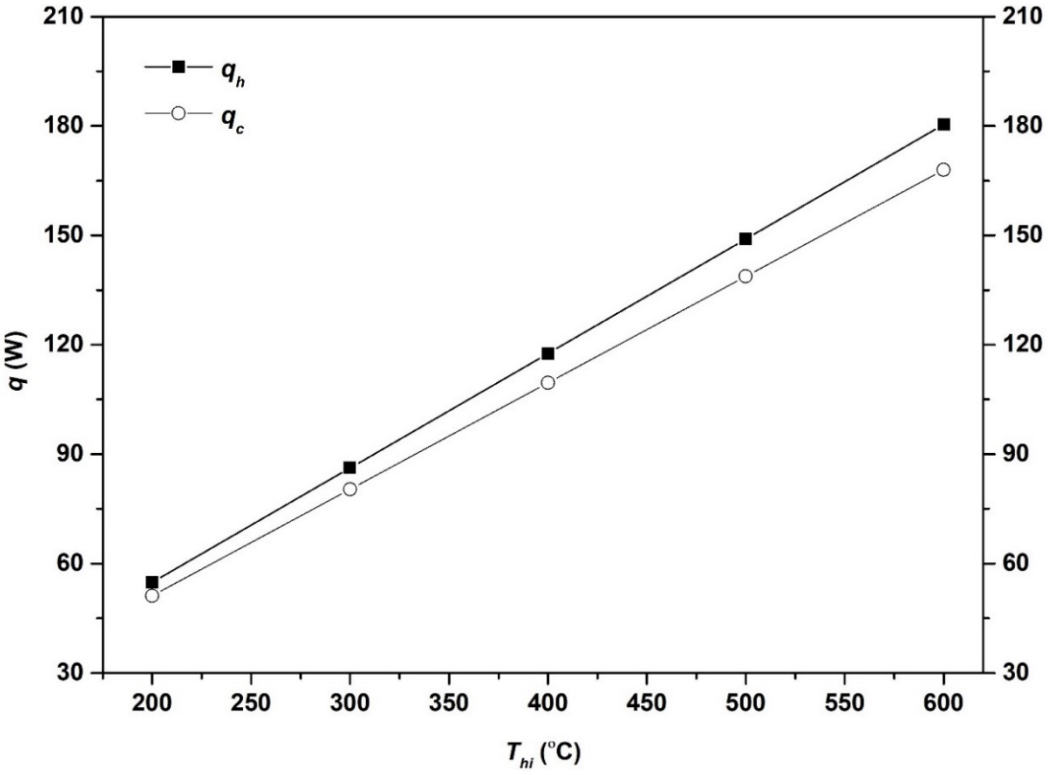

Figure 8. $\dot{q}_h$ and $\dot{q}_c$ with respect to T_{hi}.

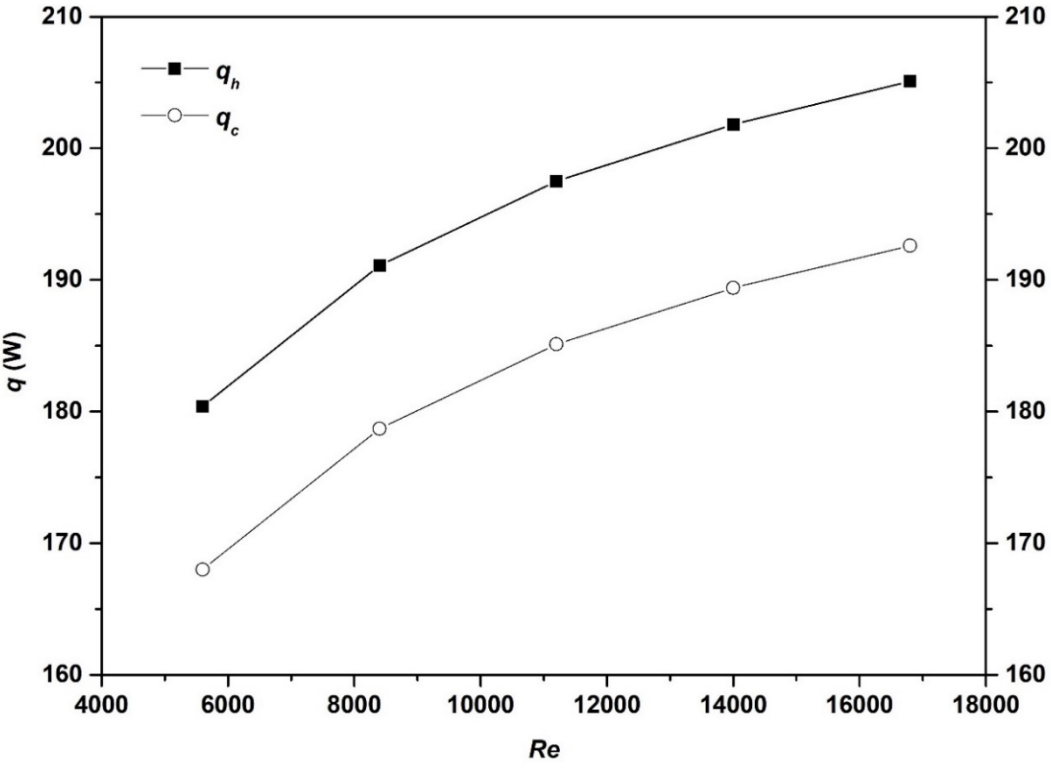

Figure 9. $\dot{q}_h$ and $\dot{q}_c$ with respect to the *Re* number.

Output power of the TEG is calculated using $P = (\dot{q}_h - \dot{q}_c)xA_{TEG}$ [20], where A_{TEG} is the total TE leg cross-sectional area of the TEG, and given in **Figure 10**. It can be seen from the figure that *P* of the TEG increase with increasing T_{hi}. According to the results, *P* values are obtained as 0.003 W, 0.005 W, 0.006 W, 0.008 W, and 0.010 W for T_{hi} of 200 °C, 300 °C, 400 °C, 500 °C, and 600 °C, respectively. As a result, maximum *P* with respect to T_{hi} of 600 °C is specified as 0.01 W. Since the A_{TEG} in this study is lower, *P* values of the TEG is lower. A_{TEG} should be increased by increasing TE leg cross-sectional area or using many pieces of TEGs to increase the output power.

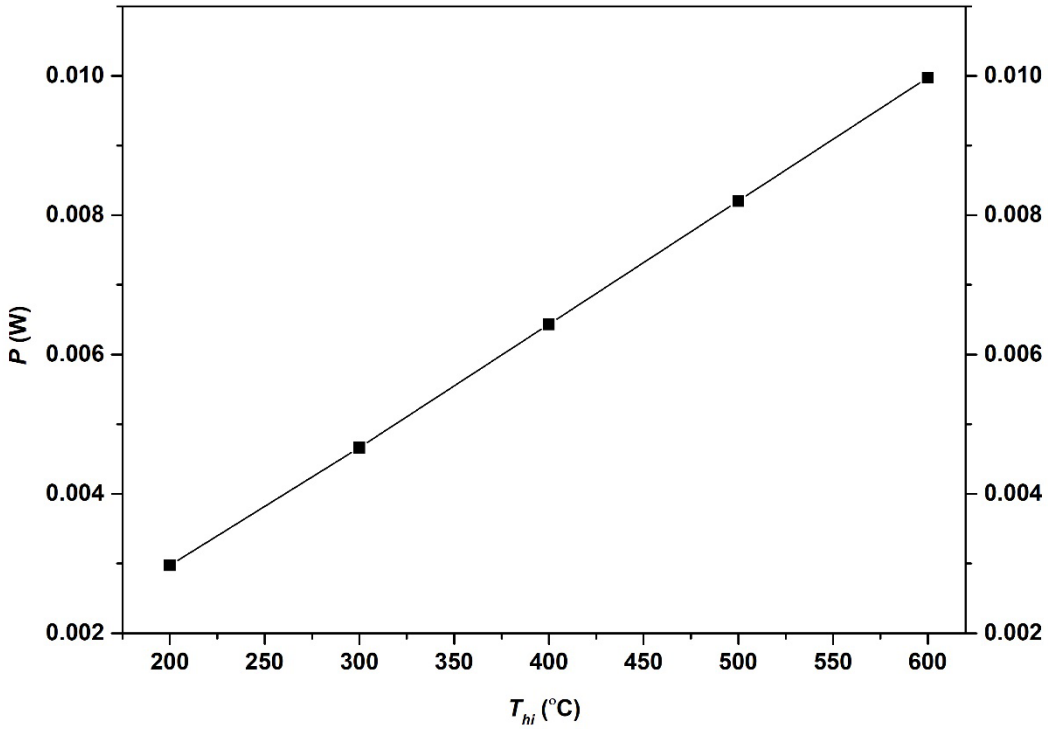

Figure 10. *P* with respect to T_{hi}.

3.5. Pressure Drop (*ΔP*)

It is important to calculate the *ΔP*, which occurs when a fluid flows through a flow system to specify additional power to manage the friction loss between the solid surfaces and the fluid. Increasing *ΔP* in TEG systems increases the net output power of the TEG systems. Within this respect, the *ΔP* between the inlet and outlet of the hot air is investigated concerning different *Re* numbers. In this study, *Re* numbers are varied as 5600, 8400, 11200, 14000, and 16800 to increase $\dot{q}_h$ and $\dot{q}_c$ and the *ΔP* results concerning *Re* numbers are illustrated in **Figure 11**. According to the figure, *ΔP* increases with increasing *Re* number in agree with the increase in the Nu number and the convection heat transfer coefficient. The increase in *ΔP* requires additional pumping power for the hot air. This situation originates from the increasing velocity of the hot air, which causes higher resistance losses. The variation in T_{hi} does not have a significant effect on the *ΔP*. As a result, the maximum and the minimum *ΔP* occur as 304.4 Pa and 36.7 Pa for the *Re* numbers of 5600 and 16800, respectively. When the *ΔP* is compared to the literature for the plate fin heat sinks, *ΔP* values are higher than the literature values [20–22]. Since the *ΔP* is calculated using $\Delta P = f\frac{L}{D}\frac{\rho V^2}{2g}$, the *ΔP* is directly related to the length (*L*) of the flow duct. In this study, *ΔP* values are higher than the literature values due to the length of the flow model. In addition, number of fins of this study is higher than the study of Kim et al. [21], which further increases the *ΔP*.

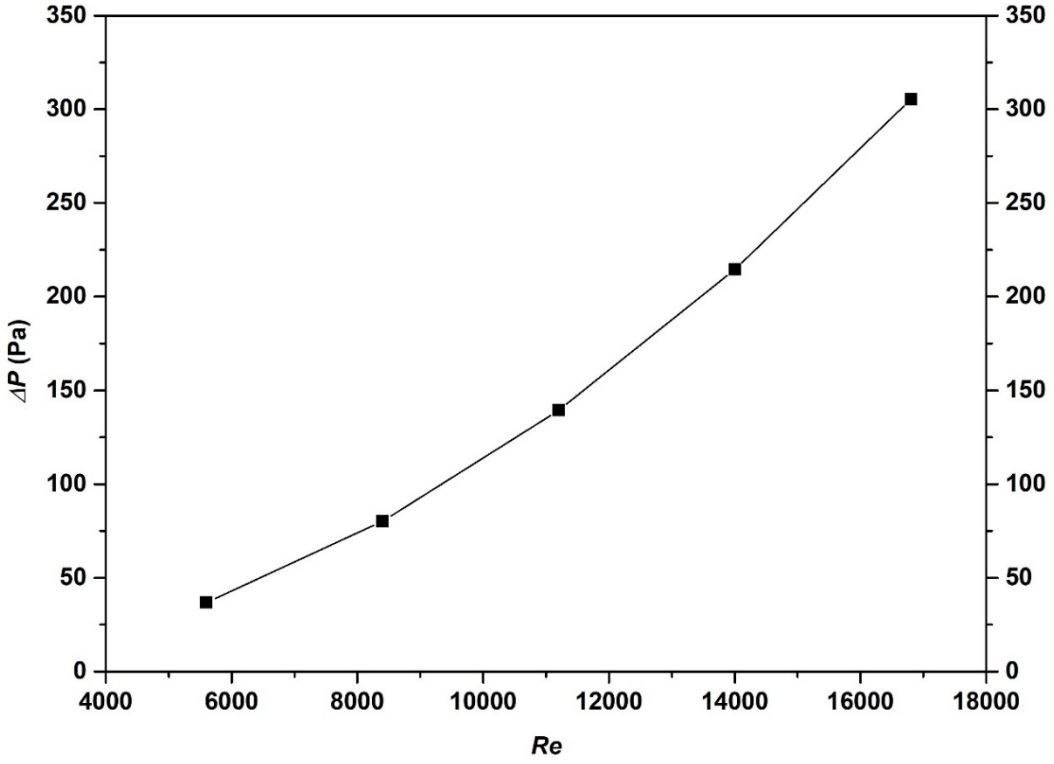

Figure 11. *ΔP* with respect to *Re* number.

T_h, T_c, ΔT, $\dot{q}_h$, $\dot{q}_c$, and ΔP of a TEG are evaluated as a result of CFD analyses to improve the output power of the TEG. The study's complete results are tabulated in **Table 2** and **Table 3** with respect to T_{hi} and *Re* number, respectively.

Table 2. T_h, T_c, ΔT, $\dot{q}_h$, and $\dot{q}_c$ of the TEG with respect to T_{hi}.

T_{hi} [°C]	T_h [°C]	T_c [°C]	ΔT [°C]	$\dot{q}_h$ [W]	$\dot{q}_c$ [W]
200	175.4	48.0	127.4	54.9	51.2
300	261.3	61.0	200.3	86.2	80.4
400	347.3	74.1	273.2	117.6	109.6
500	433.2	87.2	346.0	149.0	138.8
600	519.2	100.3	418.9	180.4	168.0

Table 3. T_h, T_c, ΔT, $\dot{q}_h$, $\dot{q}_c$, and ΔP of the TEG with respect to *Re*.

Re	T_h [°C]	T_c [°C]	ΔT [°C]	$\dot{q}_h$ [W]	$\dot{q}_c$ [W]	ΔP
5600	519.2	100.3	418.9	180.4	168.0	36.8
8400	532.6	88.0	444.6	191.1	178.7	80.1
11200	540.6	80.7	459.9	197.5	185.1	139.4
14000	546.0	75.6	470.4	201.8	189.4	214.5
16800	550.0	71.9	478.1	205.1	192.6	305.3

4. Conclusion

Steady-state numerical heat transfer analyses on both sides of a TEG were conducted using CFD to improve the power generation performance. Effects of T_{hi} and Re numbers are investigated to increase ΔT, $\dot{q}_h$, $\dot{q}_c$, and ΔP of the TEG. T_{hi} is altered as 200 °C, 300 °C, 400 °C, 500 °C, and 600 °C, while the Re number for the hot and cold air is varied as 5600, 8400, 11200, 14000, and 16800. The TEG model consists as the TEG will be between two heat sinks through which hot and cold air flows as turbulent to recover the waste heat of the hot air. When the temperature distributions through the hot and cold air are investigated, T_{hi} decreases when the hot air flows through the heat sink, while T_{ci} increases when the cold air flows through the heat sink. As a result, temperature of the hot air at the outlet of the heat sink increased and reached to the value of 598 °C, while temperature of the cold air at the outlet of the heat sink decreased to 27 °C for T_{hi} = 600 °C and Re = 16800. When the velocity distributions in the hot and cold air are investigated, velocities of the hot and cold air increases when the Re number increases and become maximum between the fins of the heat sinks. The velocities of the hot and cold air increase up to 10 m/s, 15 m/s, 20 m/s, 25 m/s, and 30 m/s, for Re numbers of 5600, 8400, 11200, 14000, and 16800, respectively.

The results show that increasing T_{hi} and Re number yields an increase in ΔT, $\dot{q}_h$, and $\dot{q}_c$. Besides, ΔP between the inlet and outlet of the hot air increases with increasing Re number. In terms of investigating ΔT, maximum T_h with respect to T_{hi} of 600 °C and Re number of 16800 is specified as 519.2 °C and 550.0 °C, respectively, while maximum ΔT is specified as 418.9 °C and 478.1 °C. Considering $\dot{q}_h$, and $\dot{q}_c$, maximum $\dot{q}_h$ with respect to T_{hi} of 600 °C and Re number of 16800 are specified as 180.4 W and 205.1 W, respectively, while the maximum $\dot{q}_c$ is specified as 168.0 W and 192.6 W. As a result of ΔP analyses, the maximum and the minimum ΔP occur as 304.4 Pa and 36.7 Pa for the Re numbers of 5600 and 16800, respectively. To improve the heat transfer rate on the hot and cold sides of the TEG, future studies could focus on the optimization of the fin geometry and number of fins for the purpose of waste heat recovery applications.

Acknowledgments

E. K., responsible for the entire article (conceptualization, literature investigation, numerical analyses, interpretation of the results, writing, editing).

References

[1] Erturun U, Erermis K, Mossi K. Influence of leg sizing and spacing on power generation and thermal stresses of thermoelectric devices. Appl. Energy 2015; 159: 19–27.
[2] Ma Q, Fang H, Zhang M. Theoretical analysis and design optimization of thermoelectric generator. Appl. Therm. Eng. 2017; 127: 758–764.
[3] Högblom O, Andersson R. A simulation framework for prediction of thermoelectric generator system performance. Appl. Energy 2016; 180: 472–482.
[4] Esarte J, Min G, Rowe DM. Modelling heat exchangers for thermoelectric generators. J. Power Sources 2001; 93: 72–76.
[5] Erturun U, Mossi K. Thermoelectric devices with rotated and coaxial leg configurations: Numerical analysis of performance. Appl. Therm. Eng. 2015; 85: 304–312.
[6] Huang K, Li B, Yan Y, Li Y, Twaha S, Zhu J. A comprehensive study on a novel concentric cylindrical thermoelectric power generation system. Appl. Therm. Eng. 2017; 117: 501–510.
[7] Liao M, He Z, Jiang C, Fan X, Li Y, Qi F. A three-dimensional model for thermoelectric generator and the influence of Peltier effect on the performance and heat transfer. Appl. Therm. Eng. 2018; 133: 493–500.
[8] Lee H, Sharp J, Stokes D, Pearson M, Priya S. Modeling and analysis of the effect of thermal losses on thermoelectric generator performance using effective properties. Appl. Energy 2018; 211: 987–996.
[9] Li W, Paul MC, Montecucco A, Siviter J, Knox AR, Sweet T, Gao M, Baig H, et al. Multiphysics simulations of thermoelectric generator modules with cold and hot blocks and effects of some factors. Case Stud. Therm. Eng. 2017; 10: 63–72.
[10] Miao Z, Meng X, Zhou S, Zhu M. Investigation for power generation based on single-vertex movement of thermoelectric module. Sustainable Cities Soc. 2020; 53: 101929.
[11] Nour Eddine A, Chalet D, Faure X, Aixala L, Chessé P. Optimization and characterization of a thermoelectric generator prototype for marine engine application. Energy 2018; 143: 682–695.
[12] Nour Eddine A, Sara H, Chalet D, Faure X, Aixala L, Cormerais M. Modeling and simulation of a thermoelectric generator using bismuth telluride for waste heat recovery in automotive diesel engines. J. Electron. Mater. 2019; 48 (4): 2036–2045.
[13] Gürbüz H, Akçay H, Topalcı Ü. Experimental investigation of a novel thermoelectric generator design for exhaust waste

heat recovery in a gas-fueled SI engine. Appl. Therm. Eng. 2022; 216 (March): 119122.
[14] Topalcı Ü, Gürbüz H, Akçay H, Demirtürk S. Buji Ateşlemeli Bir Motorda Egzoz Atık Isı Geri Kazanımı İçin Termoelektrik Jeneratör Modelinin Geliştirilmesi. Mühendislik Bilimleri ve Tasarım Dergisi 2020; 8 (2): 582–596.
[15] Kunt MA, Gunes H. An experimental study on design and performance of a waste heat recovery system with a thermoelectric generator to be used in exhaust systems of motorcycle engines. Proceedings of the Institution of Mechanical Engineers, Part E: J. Process Mech. Eng. 2021; 236 (3): 779–789.
[16] Schwurack R, Unz S, Beckmann M. The Importance of considering parasitic heat losses when modeling teg performance for high-temperature applications. J. Electron. Mater. 2019; 48 (4): 1917–1925.
[17] Akçay H, Gürbüz H, Demirtürk S, Topalcı Ü. Tipik Bir Buji Ateşlemeli Motorda Egzoz Atık Isısı Enerjisinin Geri Kazanımı İçin Geliştirilen Termoelektrik Jeneratörün HAD Analizi. El-Cezeri Fen ve Mühendislik Dergisi 2020; (3): 1088–1100.
[18] Ökmen AB, Gürbüz H. CFD analysis of optimum exhaust heat exchanger arrangement in thermoelectric generator designed for exhaust waste heat recovery of spark ignition engine. El-Cezeri J. Sci. Eng. 2021; 8 (2): 1060–1080.
[19] Wang Y, Dai C, Wang S. Theoretical analysis of a thermoelectric generator using exhaust gas of vehicles as heat source. Appl. Energy 2013; 112: 1171–1180.
[20] Chen WH, Wang CM, Huat Saw L, Hoang AT, Bandala AA. Performance evaluation and improvement of thermoelectric generators (TEG): Fin installation and compromise optimization. Energ. Convers. Manage. 2021; 250 (October): 114858.
[21] Kim TY, Lee S, Lee J. Fabrication of thermoelectric modules and heat transfer analysis on internal plate fin structures of a thermoelectric generator. Energ. Convers. Manage. 2016; 124: 470–479.
[22] Zhou F, Catton I. Numerical evaluation of flow and heat transfer in plate-pin fin heat sinks with various pin cross-sections. Numer. Heat Tr. A-Appl. 2011; 60 (2): 107–128.